Materials Research Express

PAPER

Stress-biased laminated composites for smooth folds in origami structures

RECEIVED
21 August 2018

REVISED
27 October 2018

ACCEPTED FOR PUBLICATION
5 November 2018

PUBLISHED
21 November 2018

V S C Chillara[1] and M J Dapino

NSF IUCRC on Smart Vehicle Concepts, Department of Mechanical and Aerospace Engineering, The Ohio State University, Columbus, OH 43210, United States of America

[1] Author to whom any correspondence should be addressed.

E-mail: chillara.1@osu.edu **and** dapino.1@osu.edu

Keywords: laminated composites, smart materials, origami structures, folding, residual stress, analytical model, reconfigurable creases

Abstract

Origami folding principles are attractive for morphing structures due to their potential for realizing drastic changes in shape. Laminated composites enable adaptive lightweight solutions for the implementation of rigid origami structures. This paper presents a strategy for the creation of smooth folds in finite-thickness laminated composites; the approach is applicable to smart folding structures with reconfigurable creases. An analytical laminated-plate model, based on strain energy minimization, is presented to calculate fold angle as a function of laminate parameters. Folds, realized as localized curvature at a crease, are modeled using piecewise displacement polynomials. Folded composites, created using prestressed elastomers with zero in-plane Poisson's ratio, are fabricated for demonstration and model validation. The calculated out-of-plane deflection of the curved creases is in agreement with measurements. A parametric study is conducted to characterize the sensitivity of fold angle and sharpness to variations in laminate modulus and thickness, crease width, and prestrain orientation. Narrow creases require higher prestress for a given fold angle than wider creases. Fold sharpness can be maximized by minimizing crease width and thickness. Anisotropy in the prestressed elastomer is a tradeoff between achieving zero in-plane Poisson's ratio for unidirectional prestress and maximizing the range of crease orientations for foldability.

1. Introduction

Origami folding techniques are attractive for morphing structures due to their potential for drastic changes in surface area. Foldable structures find applications in the aerospace [1, 2] and automotive [3] industries, robotics [4], and bio-inspired systems [5]. Origami design, involving the calculation of crease pattern and folding sequence, is well understood in surfaces with zero thickness [6, 7]. However, implementation of these folding principles in morphing panels with finite thickness adds functional challenges related to foldability, structural integrity, and self-folding ability [8].

In laminated composites with finite thickness, folding is typically realized as localized flexure about a crease line. The crease has finite width and its stiffness is typically much lower than that of its rigid adjacent faces; flexural stiffness of the crease is a function of its modulus and thickness. Other approaches for creating creases include the use of surrogate mechanisms such as lamina-emergent compliant joints [9]. Traditional fiber-reinforced polymeric composites are not suitable for origami folding because the fibers in a stiff matrix break upon bending [10]. Composites with a soft matrix, however, can be folded since the fibers undergo micro-buckling [11]. There is a growing interest in the area of adaptive laminated composites that are folded by creating a strain mismatch between the active and passive layers [12].

Smart materials with controllable stress-states are candidates for laminae that can provide actuation and rigidization. Shape memory alloys (SMA) and polymers (SMP) have been successfully employed as active laminae for folding sheets with pre-defined creases. Self-folding SMA sheets are achieved by locally activating an

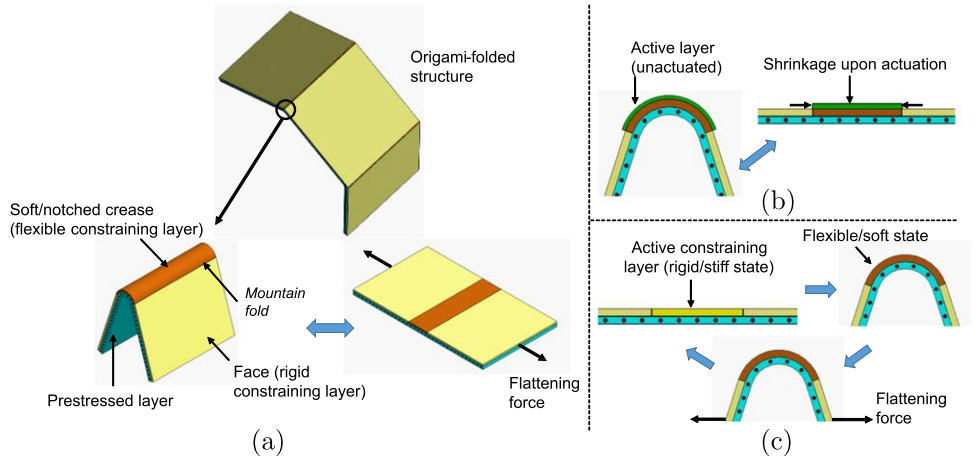

Figure 1. (a) Folds in an origami structure using prestressed laminae. Actuation of origami folds using active laminae that can (b) shrink to unfold the composite or (c) soften to fold the composite.

SMA film or mesh; the film contracts on heating and causes flexure [13]. While SMA-based designs enable two-way folding and reprogrammable shapes, the stiffness of the hinge is limited by the low bending stiffness of the SMA film. Felton *et al* [14] combined layers of SMP with pre-creased paper to form a bimorph actuator. The SMP, when activated locally using resistive circuits, shrinks to create a fold. The folded shapes can be rigidized by cooling the SMP below its glass transition temperature. Ahmed *et al* [15] demonstrated folding in electroactive polymers. The polymers contract under an applied electric field creating flexure because they are bonded to an inextensible substrate. Von Lockette *et al* [16] demonstrated notched composites that are folded by applying a magnetic field. Li and Wang [17] developed 3D origami structures in which layers of fluid were used for deployment or stiffening of the structure. Zirbel *et al* [18] presented several mechanical means to deploy an origami solar array that include torsional springs, cables, and bistable strips in the structure.

One-way actuation is sufficient for shape morphing when there is an intrinsic restoring mechanism in the composite. In fiber-reinforced polymeric composites, incorporation of intrinsic restoring stresses has been an effective approach for developing bistability [19]. Chillara *et al* [20] developed stress-biased curved composites that have an irreversible non-zero stress-state; select layers are laminated in a pre-stretched condition to create a stress bias that manifests as curvature in the composite. Stress-biased composites are attractive for folding because the built-in spring enables the structure to remain folded in the unactuated state [21]. Prior literature has covered self-folding and intrinsic stress, but there is a need to investigate structures that incorporate both.

This paper presents a strategy for combining smart actuation and intrinsic stress to create reconfigurable folds in laminated composites. The benefits of this strategy are as follows: deformation can be programmed using the intrinsic spring force; the unactuated composite has a folded shape that can be flattened using a single actuator; and prestress can be restricted to specific laminae to enable the addition of layers that provide controllable stiffness or actuation. The resulting smart composite can serve multiple functions such as structural integrity, built-in actuation, and shape reconfiguration.

To illustrate the folding strategy, a creased constraining layer is laminated to a prestressed layer (figure 1(a)). A constraining layer is flexible but has high in-plane modulus relative to the prestressed layer. The modulus or thickness of the constraining layer in the creased region is much lower than that of the faces. A prestressed layer is stretchable and is laminated in the stretched state to a constraining layer with one or more creases. The direction of prestress can be at a non-zero angle relative to the crease line. In origami terminology, prestressed composites exhibit mountain folds at equilibrium. In a structure with both mountain and valley folds, a minimum of two prestressed layers, one on either face of a creased constraining layer, is required to fold all creases.

A folded prestressed composite can be flattened through the contraction of a smart lamina at a crease (figure 1(b)). Upon deactivation, the composite returns to its folded shape. Another actuation approach involves the localized softening of a stiff fold-free smart material-based constraining layer to form a flexible crease (figure 1(c)). The composite folds about the softened region (crease) due to the intrinsic mechanical prestress. These folding strategies enable actuator reduction because multiple creases can be simultaneously unfolded using an external force field applied to the structure. This paper addresses research questions related to prestress-based folding through: determination of the effect of magnitude and orientation of prestress on fold angle; determination of the effect of crease width, modulus, and thickness on fold angle and sharpness; and

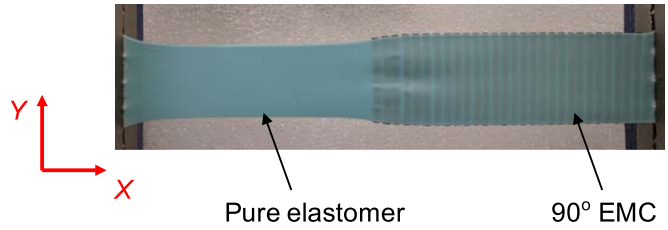

Figure 2. Elastomeric matrix composite (EMC) strip partially reinforced with fibers along its width to demonstrate near-zero in-plane Poisson's ratio.

establishment of a mathematical relationship between prestress and fold geometry in origami folds with curved faces.

Mechanical prestress in folded composites provides several additional design possibilities. For example, curved faces can be created in a folded structure by extending the prestressed laminae onto the faces. This feature is particularly useful in the folding of curved shells [22, 23]. Prestress also enables bistability [24] in the fold faces and in the folded structure. Origami tessellations such as Miura-Ori could serve as a constraining layer, resulting in metamaterial characteristics. A prestressed layer can not only enable folds, but also serve as a stretchable skin on a morphing structure. Therefore, a mechanically-prestressed composite structure is capable of multiple morphing modes like stretching, flexure, and folding, while serving multiple functions such as structural integrity, bistability, and shape reconfiguration.

A method for the fabrication of a passive folded composite is presented in section 2. An analytical model based on laminated-plate theory is developed to characterize the fold angle at a crease with relatively rigid faces (section 3). Composite displacements are defined using piecewise functions to accurately describe the large localized out-of-plane deflection associated with a folded crease. Model-based simulations of the folded shapes with flat and curved faces are presented in section 4. Parametric studies are conducted to characterize the sensitivity of fold angle to the material properties and dimensions of the crease, and the magnitude and orientation of the applied prestrain. Conclusions are discussed in section 5.

2. Composite fabrication

A method for the fabrication of mechanically-prestressed folded composites is presented in this section. Creases of various widths are fabricated to demonstrate the influence of crease width on fold angle and to validate the analytical model.

2.1. Elastomeric matrix composites

In this work, folded composites are created by laminating prestressed fiber-reinforced elastomers and a creased constraining layer. Figure 2 shows an elastomer comprising silicone rubber reinforced with unidirectional carbon fibers; reinforced elastomers are also known as elastomeric matrix composites (EMC). The EMC shown in figure 2 is prestressed in the X direction. A portion of this EMC is reinforced with fibers in the Y direction. Addition of fibers in this 90° orientation restricts the change in width to yield near-zero in-plane Poisson's ratio in contrast to a reduction in width in the isotropic portion due to a high Poisson's ratio of 0.4–0.5. Murray *et al* [25] and Bubert *et al* [26] have demonstrated 90° EMCs for one-dimensional morphing of an aircraft wing. For prestressed composites, the EMCs are fabricated by sandwiching unidirectional carbon fibers between a pair of pre-cured silicone rubber sheets. The design details and the constitutive response of the 90° EMC considered in this work are the same as presented by Chillara *et al* [20].

2.2. Folds

Figures 3(a) and 3(b) show a composite that is folded at its crease by laminating a mechanically-prestressed layer. The constraining layer is a silicone rubber skin (durometer grade 45 A) reinforced with a single layer of woven carbon fabric. Rigid faces are created by laminating 0.127 mm thick spring steel shims to the constraining layer (figure 3(b)). The faces have a square geometry with a side length of 76.2 mm. The width of the crease is 19 mm. A 90° EMC of width 38.1 mm is stretched by 25% and is laminated over the length of the constraining layer. Soft materials reinforced with woven fibers not only serve as a constraining layer due to their high in-plane stiffness, but also mitigate the shear stress between a highly-stretched elastomer and a relatively inextensible material such as steel. The prestressed composite exhibits a fold through large curvature at the crease. The faces are also curved due to prestress, but the face curvature is much smaller than the crease curvature because the additional

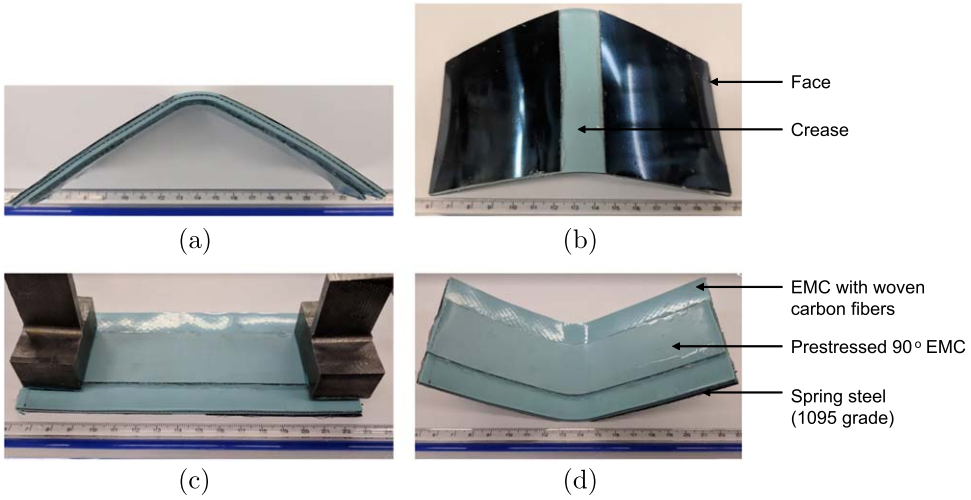

Figure 3. Stress-biased (prestressed) folded composite: (a) top and (b) front views; (c) unfolded shape; and (d) folded shape.

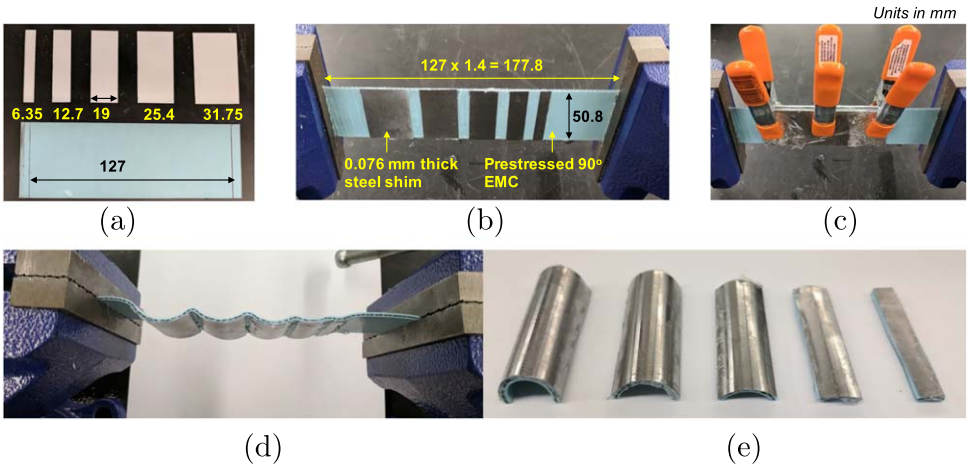

Figure 4. (a) A 90° EMC and creases cut out of 0.0762 mm thick steel shim; (b) steel shims laminated to a prestressed 90° EMC; (c) curing of the laminate under applied pressure; (d) composite shape after removal of prestress; (e) curved creases obtained from trimming the composite in (d).

constraining steel layer provides higher bending stiffness on the faces. Figures 3(c) and 3(d) show the unfolded and folded shapes, respectively. In the unactuated state, or in the absence of external forces, the composite has a folded stable shape. The interior angle between the faces is measured to be 120°.

To examine the effect of crease width, pure creases with widths ranging from 6.35 mm to 31.75 mm are laminated to a prestressed EMC as shown in figure 4(a). Steel shims represent the constraining layer and they are laminated to the same EMC to minimize variation in input prestress between samples (figure 4(b)). The laminated composite, shown in figure 4(c), is cured under pressure for 24 h. The shape of the composite after removal of prestress is shown in figure 4(d). By inspection, the out-of-plane deformation increases with an increase in crease width. Curvature was measured to be the same in all samples. This is consistent with Chillara and Dapino's [24] modeling results that indicate that, for a given EMC prestrain, curvature is independent of the characteristic length of a rectangular composite. Figure 4(d) provides an example for stretchable composites with localized curvature and folds. To eliminate end-effects in measurement, the creases are trimmed from the EMC and their curvature is measured (figure 4(e)).

3. Analytical model

The elastic behavior of origami structures has been modeled by treating the folds as 1-D revolute joints with a finite stiffness [27]. A common approach to modeling the curved shapes of composites is to formulate strains using laminated-plate theories and calculate the deformations using strain energy minimization [28–30]. Using

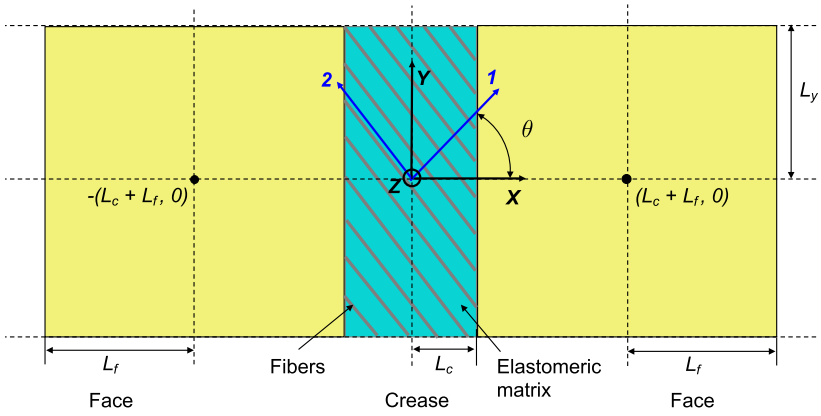

Figure 5. Schematic of a prestressed creased composite for modeling.

this approach, Peraza-Hernandez *et al* [31] studied the structural mechanics of creases with non-zero width. Their modeling effort included a simplified strain energy-based numerical model that assumes zero in-plane strain and constant curvature. In practice, there is finite in-plane strain and curvature is not constant since the faces adjacent to a crease act as elastic boundary conditions. The boundary effects due to the relatively stiff faces are significant when prestress is not orthogonal to the crease line. Mattioni *et al* [32] presented a piecewise-displacement model to calculate the curved shapes of bistable composites with elastic boundary conditions. The existing structural mechanics models are suitable for calculating the shape of a pure crease but not of a crease with adjacent flat or curved faces.

In this work, a folded composite is modeled in its most basic form as a structure that comprises two faces joined by a crease (figure 5). A fold is characterized by large curvature at the crease relative to the face. Strains are modeled per classical laminate theory in conjunction with von Karman's hypothesis [30]. Strain energy is minimized to calculate the folded shape. Curvature at the crease is modeled using displacement functions that can be described using polynomials [24, 28]. Globally-defined polynomial functions yield poor accuracy and numerical ill-conditioning for the modeling of highly localized curvature as is the case with folded structures. Therefore, a piecewise definition of polynomials is used across the crease and the adjacent faces to describe a folded shape.

3.1. Composite strains

The composite is modeled as three sections that correspond to one crease and two adjacent faces (figures 5 and 7). The constraining layer is assumed to be a material whose modulus can be controlled in the creased region. Composite strains are expressed in terms of the displacement (u, v, w) of an arbitrary point (x, y, z) on the composite as:

$$\epsilon_{xx} = \frac{\partial u}{\partial x} + \frac{1}{2}\left(\frac{\partial w}{\partial x}\right)^2, \tag{1}$$

$$\gamma_{xy} = \frac{\partial u}{\partial y} + \frac{\partial v}{\partial x} + \frac{\partial w}{\partial x}\frac{\partial w}{\partial y}, \tag{2}$$

$$\epsilon_{yy} = \frac{\partial v}{\partial y} + \frac{1}{2}\left(\frac{\partial w}{\partial y}\right)^2. \tag{3}$$

Displacements (u, v, w) are written in terms of mid-plane displacements (u_0, v_0, w_0) as:

$$u(x, y, z) = u_0(x, y) - z\frac{\partial w_0(x, y)}{\partial x}, \tag{4}$$

$$v(x, y, z) = v_0(x, y) - z\frac{\partial w_0(x, y)}{\partial y}, \tag{5}$$

$$w(x, y, z) = w_0(x, y). \tag{6}$$

The geometric mid-plane is located based on the maximum thickness H (figure 7). Strain of an arbitrary plane z is obtained by substituting (4)–(6) into (1)–(3):

$$\epsilon_x = \frac{\partial u_0}{\partial x} + \frac{1}{2}\left(\frac{\partial w_0}{\partial x}\right)^2 - z\left(\frac{\partial^2 w_0}{\partial x^2}\right), \tag{7}$$

$$\gamma_{xy} = \frac{\partial u_0}{\partial y} + \frac{\partial v_0}{\partial x} + \frac{\partial w_0}{\partial x}\frac{\partial w_0}{\partial y} - 2z\left(\frac{\partial^2 w_0}{\partial y \partial x}\right), \tag{8}$$

$$\epsilon_y = \frac{\partial v_0}{\partial y} + \frac{1}{2}\left(\frac{\partial w_0}{\partial y}\right)^2 - z\left(\frac{\partial^2 w_0}{\partial y^2}\right). \tag{9}$$

Prestrain in an EMC is applied in the direction orthogonal to fiber-orientation in order to maintain zero in-plane Poisson's ratio. Fold angle is expected to be maximum and minimum when the direction of prestrain is perpendicular and parallel to the crease, respectively. Modeling the relationship between fold angle and prestrain orientation provides insight into the design of multiple non-parallel folds using a single prestressed EMC. Assuming a plane stress condition, strain in the material coordinates of an EMC (*1-2* axes in figure 5) is written in terms of composite strain as:

$$\begin{Bmatrix} \epsilon_1 \\ \epsilon_2 \\ \epsilon_6 \end{Bmatrix} = \begin{bmatrix} \cos^2\theta & \sin^2\theta & \sin\theta\cos\theta \\ \sin^2\theta & \cos^2\theta & -\sin\theta\cos\theta \\ -2\sin\theta\cos\theta & 2\sin\theta\cos\theta & \cos^2\theta - \sin^2\theta \end{bmatrix} \begin{Bmatrix} \epsilon_x \\ \epsilon_y \\ \gamma_{xy} \end{Bmatrix}, \tag{10}$$

where θ is the angle between the X axis and the direction of the applied prestrain (1 axis).

3.2. Strain Energy Function

The total strain energy (Φ) can be expressed in terms of the strain energy of the crease (Φ_c), faces (Φ_f), and the prestressed EMC (Φ_e) as:

$$\Phi = \Phi_c + \Phi_f + \Phi_e. \tag{11}$$

The strain energy of a crease is:

$$\Phi_c = \int_{-L_c}^{L_c}\int_{-L_y}^{L_y}\int_{h_1}^{h_2}\left(\frac{1}{2}\bar{Q}_{11}^{(c)}\epsilon_x^2 + \bar{Q}_{12}^{(c)}\epsilon_x\epsilon_y + \frac{1}{2}\bar{Q}_{22}^{(c)}\epsilon_y^2 + \frac{1}{2}\bar{Q}_{66}^{(c)}\gamma_{xy}^2\right)\mathrm{d}z\ \mathrm{d}y\ \mathrm{d}x, \tag{12}$$

where $\bar{Q}_{ij}$ $(i,j = 1,2,6)$ are the plane stress-reduced stiffness parameters [30]. The strain energy integrand of a face is written as:

$$\mathrm{d}\Phi_f = \int_{h_1}^{H/2}\left(\frac{1}{2}\bar{Q}_{11}^{(f)}\epsilon_x^2 + \bar{Q}_{12}^{(f)}\epsilon_x\epsilon_y + \frac{1}{2}\bar{Q}_{22}^{(f)}\epsilon_y^2 + \frac{1}{2}\bar{Q}_{66}^{(f)}\gamma_{xy}^2\right)\mathrm{d}z. \tag{13}$$

The strain energy of the faces is written in terms of $\mathrm{d}\Phi_f$ as:

$$\Phi_f = \int_{-(L_c+2L_f)}^{-L_c}\int_{-L_y}^{L_y}\mathrm{d}\Phi_f\ \mathrm{d}y\ \mathrm{d}x + \int_{L_c}^{(L_c+2L_f)}\int_{-L_y}^{L_y}\mathrm{d}\Phi_f\ \mathrm{d}y\ \mathrm{d}x. \tag{14}$$

The thickness of the crease and face is $(h_2 - h_1)$ and $(H/2 - h_1)$, respectively. The condition $h_2 > h_1$ always holds. The strain energy of a 90° EMC that has a prestrain of ϵ_{90} across the crease is:

$$\begin{aligned}\Phi_e = \int_{-L_c}^{L_c}\int_{-L_y}^{L_y}\int_{-H/2}^{h_1}\Bigg(&\frac{p_1}{5}(\epsilon_{90}-\epsilon_1)^5 + \frac{p_2}{4}(\epsilon_{90}-\epsilon_1)^4 \\ &+ \frac{p_3}{3}(\epsilon_{90}-\epsilon_1)^3 + \frac{p_4}{2}(\epsilon_{90}-\epsilon_1)^2 + \frac{1}{2}Q_{22}^{(90)}\epsilon_2^2 + \frac{1}{2}Q_{66}^{(90)}\gamma_6^2\Bigg)\mathrm{d}z\ \mathrm{d}y\ \mathrm{d}x.\end{aligned} \tag{15}$$

Note that the areal dimensions of an EMC can be modified to model cases where the EMC extends onto the faces. The coefficients p_1 through p_4 in (15) correspond to a nonlinear constitutive equation that describes the material response of a 90° EMC in the prestressed direction; the EMC comprises silicone rubber reinforced with 17% by volume of unidirectional carbon fibers. The stress-strain curve is obtained from a uniaxial tensile test [20]. The values of the coefficients are listed in table 1.

The in-plane Poisson's ratio of the prestressed 90° EMC is assumed to be zero. Assuming that the modulus of carbon fiber and silicone rubber (assumed linear up to 20% strain) is 240 GPa and 1.2 MPa, respectively, transverse modulus E_2 is calculated per the rule of mixtures [30] to be 40.8 GPa. For the chosen EMC thickness of 2mm, this calculated value of E_2 corresponds to a high bending stiffness and is hence a poor approximation for a flexible EMC; evidence for the EMC's flexibility in the fiber-direction is found in figure 3(d) where the woven-fiber-reinforced EMC is seen to be flexible at the crease.

Tensile tests conducted in the fiber-direction for the measurement of E_2 resulted in slippage at the gripping points between the fibers and the matrix at small strains. Accurate measurement of E_2 was obtained through a fiber-pull-out test conducted in a tensile testing machine. Unidirectional carbon fibers (3.1 kg m^{-2}, Fiberglast Developments Corp.), oriented in the direction of vertical motion of the test frame, are pulled out of silicone

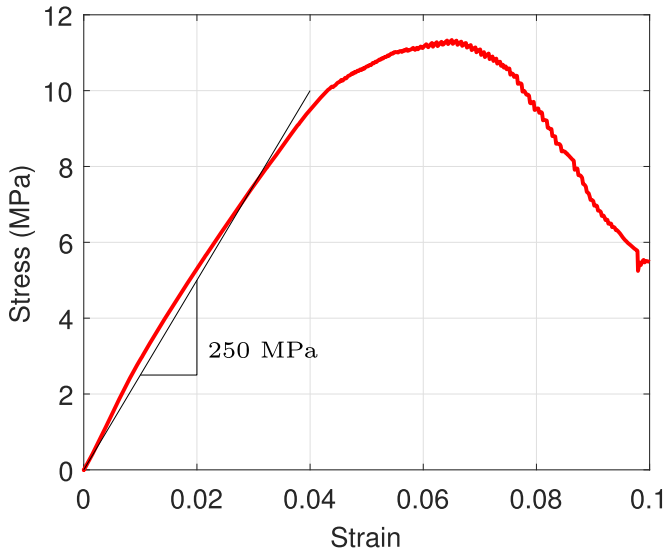

Figure 6. Stress-strain curve recorded from a fiber pull-out test conducted on an EMC comprising silicone rubber reinforced with undirectional carbon fibers.

Table 1. Polynomial coefficients of a nonlinear stress function of an EMC with zero in-plane Poisson's ratio, obtained from a uniaxial tensile test [20].

p_1	p_2	p_3	p_4
-0.698×10^6	2.29×10^6	-2.306×10^6	1.598×10^6

rubber (Rhodorsil V340-CA45). The dimensions of the rectangular test sample are $50.8 \times 19 \times 2$ mm. From the measured stress strain response, shown in figure 6, the effective transverse modulus for small in-plane strain (under 4%) is calculated to be 250 MPa. The shear modulus of a 90° EMC is assumed to be 1.2 MPa, which is $0.8 \times E_1$ per Murray *et al* [25]; the average value of E_1 is 1.5 MPa for a strain of up to 20%. The transverse and shear moduli are used to calculate $Q_{22}^{(90)}$ and $Q_{66}^{(90)}$, respectively.

3.3. Computation of fold angle

Mid-plane displacements of the composite are described by polynomial functions as:

$$u_0 = \sum_{j=0}^{O_i} \sum_{i=0}^{q} b_{i,j-i} x^i y^{i-j}, \tag{16}$$

$$v_0 = \sum_{j=0}^{O_i} \sum_{i=0}^{q} c_{i,j-i} x^i y^{i-j}, \tag{17}$$

$$w_0 = \sum_{j=0}^{O_i} \sum_{i=0}^{q} d_{i,j-i} x^i y^{i-j}, \tag{18}$$

where O_i is the order of the piecewise polynomials chosen to describe the shape of the crease and faces based on the expected deformed shape. Shape functions described by $b_{i,j-i}$, $c_{i,j-i}$, and $d_{i,j-i}$ of the crease and faces are calculated through strain energy minimization. The x limits of the functions defining the crease are $\{-L_c, L_c\}$. Similarly, the limits for the left and right faces are $\{-L_c - 2L_f, -L_c\} \cup \{L_c, L_c + 2L_f\}$. The geometric constraints that couple the crease and the faces correspond to the edge interface at $(-L_c, y)$ and (L_c, y). The constraints are defined as follows:

$$u_0^{(c)} = u_0^{(f)}, \quad v_0^{(c)} = v_0^{(f)}, \quad w_0^{(c)} = w_0^{(f)}, \quad \frac{\partial w_0^{(c)}}{\partial x} = \frac{\partial w_0^{(f)}}{\partial x}, \tag{19}$$

where the superscripts c and f denote the crease and faces, respectively. Specific symmetry conditions can be used to simplify the displacement polynomials. Example cases are discussed in section 4. The total potential energy is minimized using the constrained optimization function *fmincon* in MATLAB to yield a set of nonlinear equations with the polynomial coefficients $b_{i,j-i}$, $c_{i,j-i}$, and $d_{i,j-i}$ as the independent variables. Fold angle at the crease is defined as the internal angle subtended by the faces at the vertex of the fold (figure 7). The inclination of

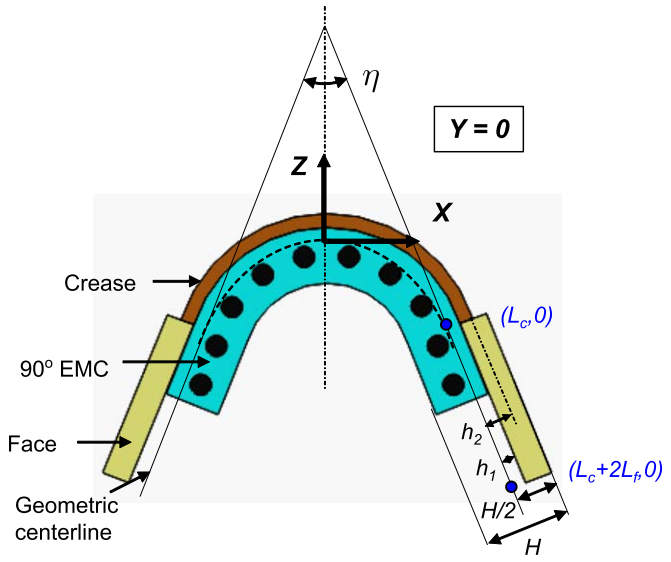

Figure 7. Schematic of a composite illustrating fold angle at the vertex of a crease.

Table 2. Geometric and material properties of the laminae for modeling.

Parameter	Steel (face)	Steel (crease)	90° EMC (face and crease)
Length (mm)	50.8 [$2L_y$]	50.8 [$2L_y$]	50.8 [$2L_y$]
Width (mm)	63.5 [$2L_f$]	19.05 [$2L_c$]	19.05 [$2L_c$]
Thickness (mm)	0.2	0.0762	2
E_1 (MPa)	2×10^5	2×10^5	Nonlinear
E_2 (MPa)	2×10^5	2×10^5	250
G_{12} (MPa)	0.78×10^5	0.78×10^5	1.2
ν_{12}	0.28	0.28	0
ν_{21}	0.28	0.28	0

each face, curved or flat, is obtained by calculating the slope of the face from the points (L_c,0) and ($L_c + 2L_f$, 0). The fold angle (η) is defined as:

$$\eta = 2\left(90 - \frac{180}{\pi}\left(\tan^{-1}\left(\frac{w_0|_{(L_c,0)} - w_0|_{(L_c+2L_f,0)}}{(L_c + u_0|_{(L_c,0)}) - (L_c + 2L_f + u_0|_{(L_c+2L_f,0)})}\right)\right)\right). \quad (20)$$

4. Results and discussion

Simulations are conducted on a composite comprising a single crease and its adjoining faces with dimensions and material properties as listed in table 2. The composite's configuration is as shown in figure 5. EMC prestrain is applied in the X direction. The folded shape of the composite is expected to be symmetric about the XZ plane whereas the deformation of the crease is expected to be symmetric about the YZ plane. By imposing symmetry conditions, the displacement polynomials are simplified per the relations listed in table 3. For folds with flat faces, the order of the polynomials for u_0, v_0, and w_0 can be reduced to 1.

4.1. Folded shapes and model validation

The composite's out-of-plane deflection is calculated for an EMC prestrain of 30% applied only across the crease (figure 8). Deformation is seen only within the region of prestress application, i.e., at the crease, while the faces remain flat. For comparison, the shape of a pure crease (without its adjoining faces) is also calculated. By inspection, the inclusion of faces has minimal effect on the out-of-plane deflection at the straight edges ($\pm L_c$, y) of the crease. The small difference in deflection can be attributed to the tangency condition imposed numerically between the crease and the face (inset in figure 8). This result is consistent with the observation by

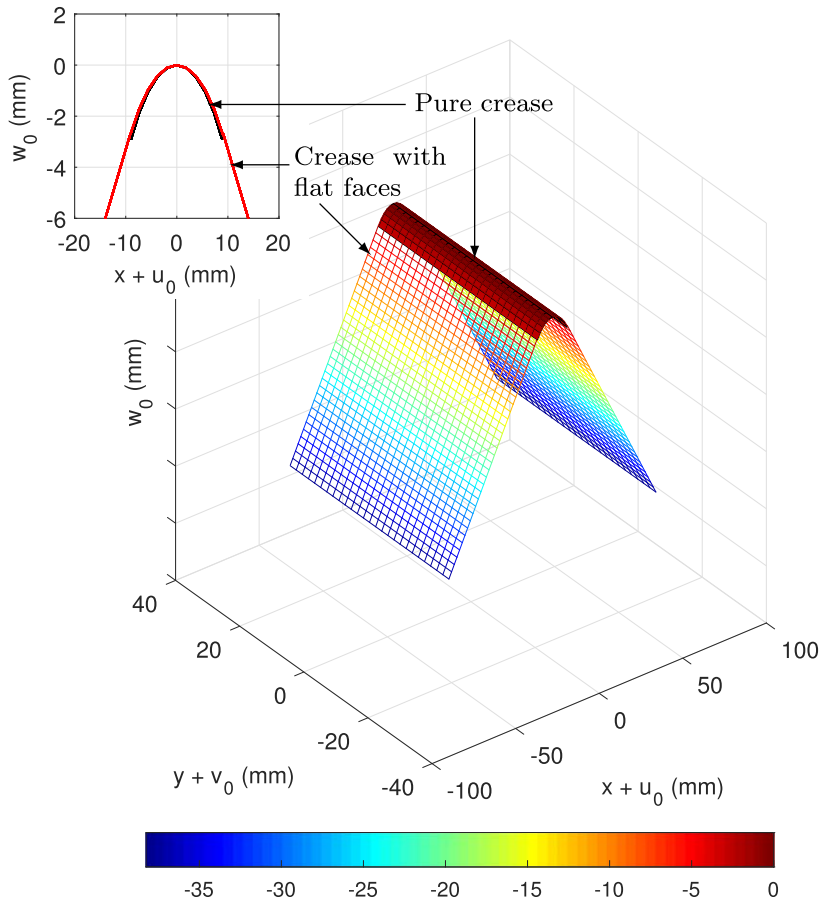

Figure 8. Comparison of the shapes of a pure crease and a crease with flat faces; the respective shapes are shown in the *XZ* plane with black and red lines.

Table 3. Conditions imposed on displacement polynomials for the modeling of folds at a crease with orthogonal EMC prestrain.

	Crease		Face	
	O_i	Condition	O_i	Condition
u_0	3	Odd in x, even in y, $u_0(0,\,0) = 0$	3	Even in y
v_0	3	Odd in y, even in x, $v_0(0,\,0) = 0$	3	Odd in y, $v_0(L_c + L_f,\,0) = 0$
w_0	4	Even in x and y, $w_0(0,\,0) = 0$	4	Even in y

Mattioni *et al* [32] that the inclusion of an elastic boundary on the straight edge of a cylindrically-curved plate has negligible impact on its curvature. Given the negligible difference between the shapes of a crease with and without the faces, the analytical model can be validated by comparing the simulated curved shapes of pure creases with the corresponding shapes of the physical specimens like those in figure 4. The crease specimens have the same curvature and hence their deformation is quantified using the out-of-plane deflection. Creases of various widths are fabricated with an EMC prestrain of 40%. The deflection of each crease is measured using a vernier caliper and found to be in agreement with the corresponding calculated values at 40% prestrain (figure 9).

Curved faces in a folded composite are created by extending the prestressed EMC lamina to cover the faces. The folded shape obtained from model-based simulations is plotted in figure 10 with reference to a fold with flat faces for a 90° EMC prestrain (ϵ_{90}) of 30%. By inspection, it is seen that the tangency constraint specified in the model is maintained at the edges common to a crease and its adjacent faces. The out-of-plane displacement at $(L_c + 2L_f,\,0)$ is higher when the faces have a convex curvature, thereby yielding a higher fold angle than in the case where the faces are flat even though the deformation at the crease is the same (inset in figure 10). Therefore, for a given EMC prestrain, fold angle is smaller in surfaces with higher initial convex curvature.

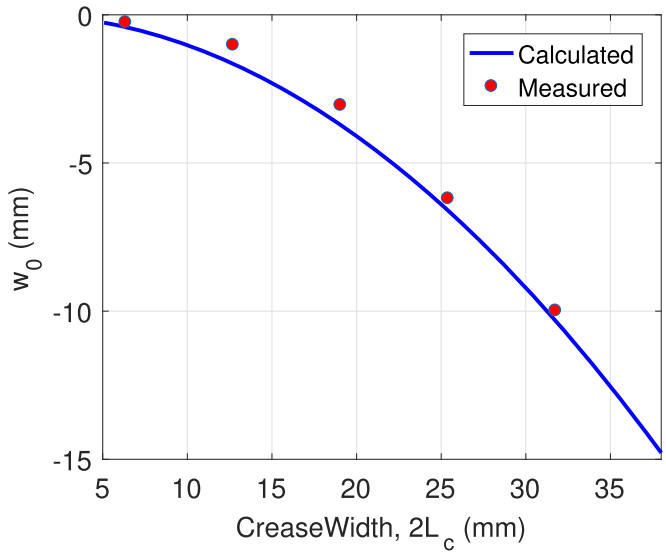

Figure 9. Out-of-plane deflection of the straight edges of a crease fabricated without the included faces. The data presented corresponds to prestrain (ϵ_{90}) of 40%.

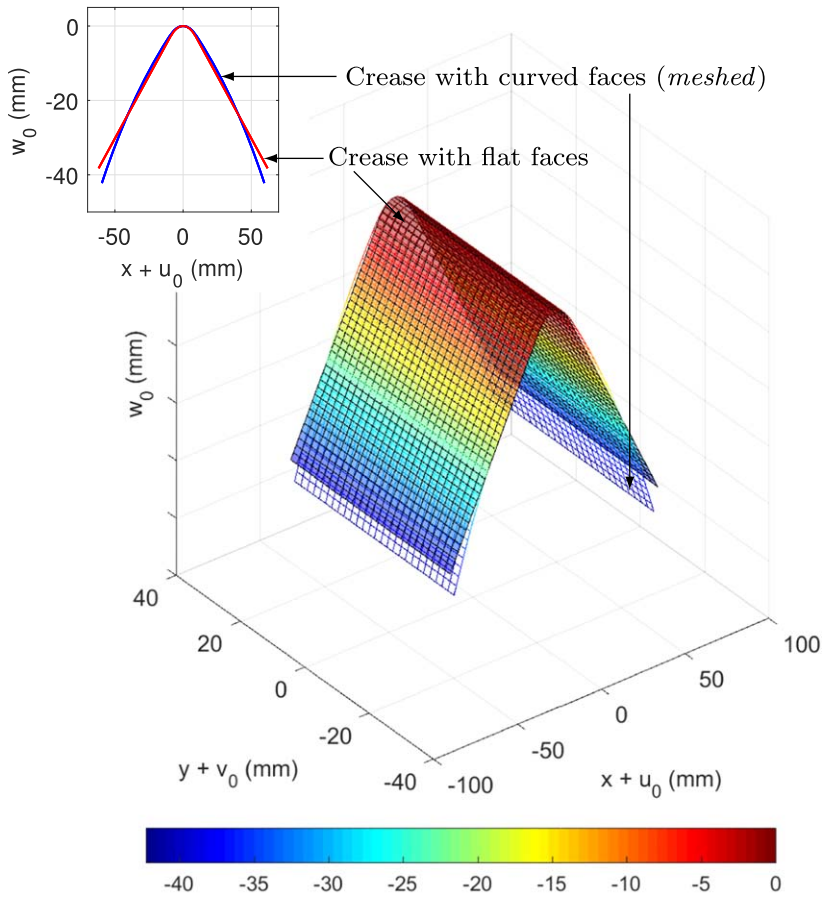

Figure 10. Comparison of fold shapes comprising a crease with flat and curved faces; the respective shapes are shown in the *XZ* plane with red and blue lines.

4.2. Model-based parametric study

4.2.1. Effect of crease width

The variation of fold angle as a function of crease width for various values of EMC prestrain is shown in figure 11. For a given EMC prestrain ϵ_{90}, fold angle decreases with an increase in crease width. Such a response, also

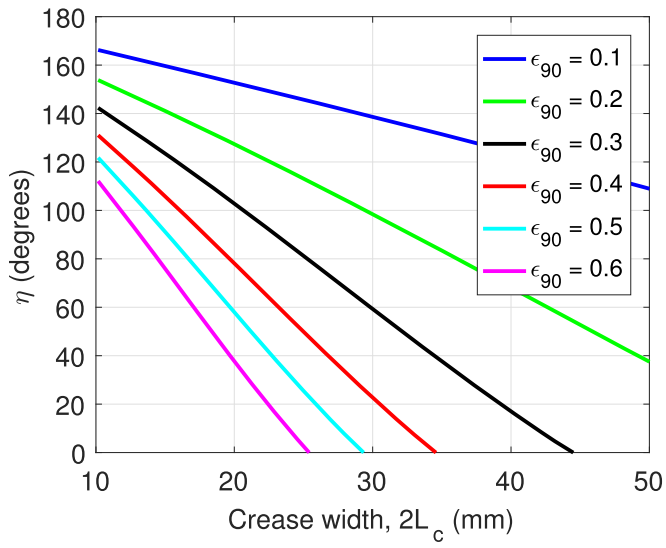

Figure 11. Fold angle as a function of crease width shown for a crease thickness and modulus of 0.003 in. (76 μm) and 200 GPa, respectively.

observed experimentally (figure 9), can be explained using the mathematical relationships between the displacement polynomials and fold angle. The out-of-plane deflection w_0 is an even monotonically increasing function of x. In-plane displacement u_0 also increases monotonically with increase in x but at a lower rate than w_0 since the polynomial u_0 is of lower order (see table 3). Therefore, from (20), η decreases with an increase in crease width since $\tan^{-1}(x)$ is an increasing function. In narrow creases, higher EMC prestrain is required to create the same fold angle as in wider creases. Further, the sensitivity of fold angle to EMC prestrain reduces with a decrease in crease width. This trend can be explained by the fact that in narrow creases, where EMC thickness is comparable to crease width, the strain energy associated with prestress manifests as high in-plane strain in the EMC. On the other hand, in wide creases the input strain energy primarily manifests as out-of-plane deformation.

4.2.2. Combined effect of crease modulus and width

Figure 12 shows the variation of fold angle as a function of crease modulus and width. For a given width of the crease, fold angle reduces exponentially with linear reduction in modulus. Fold angle is more sensitive to modulus change in wide creases as compared to narrow creases. Fold limit can be maximized by maximizing width and minimizing modulus. However, crease width may be limited by the required scale and resolution of folds in an origami structure. Folding can be achieved by actively softening the crease. This actuation approach can be realized using smart materials with controllable modulus such as SMAs [33] and SMPs [34], magnetorheological materials [35], and phase change materials [36]. Fold angle reduces upon softening of the crease due to the intrinsic restoring force in the prestressed EMC. For example, an SMA crease, laminated with a prestressed EMC in its twinned Martensite phase, can fold by undergoing detwinning; elastic modulus of detwinned Martensite is about 25 GPa. The composite can be unfolded by heating the SMA to the Austenite phase (modulus of about 75 GPa). The range of folding that may be achieved using SMA creases is indicated using planes in figure 12.

4.2.3. Combined effect of crease thickness and width

Fold sharpness (Ω) is defined in terms of fold angle (η), crease thickness ($t = h_2 - h_1$), and width ($2L_c$) as follows:

$$\Omega = \frac{\eta}{2L_c t}. \tag{21}$$

Figure 13 shows the variation of fold sharpness as a function of crease width and thickness, calculated for a crease modulus of 2 GPa. EMC prestrain is maintained constant at 30%. For a given thickness, Ω reduces exponentially with an increase in crease width. At constant crease width, sharpness can be increased by reducing crease thickness up to a critical value. Below this critical t, the composite is completely folded, i.e., $\eta \to 0$. Therefore, lowering t below the critical value does not yield a higher Ω. Fold sharpness can be maximized by minimizing crease width and thickness. It is emphasized that the composite's thickness can also be lowered by reducing the EMC's thickness, thereby increasing fold sharpness. However, a reduction in EMC thickness

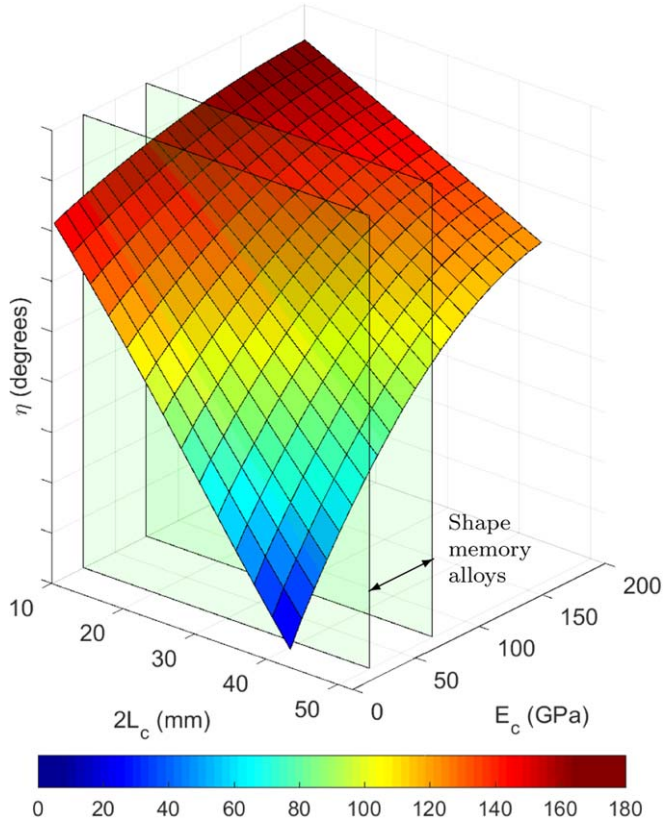

Figure 12. Fold angle as a function of crease modulus and width at a constant thickness of 0.003 in. (76.2 μm). The modulus range for shape memory alloys is illustrated as an example for the selection of materials with controllable modulus.

corresponds to a reduction in the strain energy associated with a given prestrain. Thin EMCs would require higher prestrain to generate a given fold angle as compared to thick EMCs.

4.2.4. Effect of EMC orientation

The orientation of EMC prestrain relative to the crease is expected to influence fold angle. In this study, displacement polynomials are chosen so as to include twist in the crease at non-orthogonal orientations of the EMC; the prestressed EMC spans only the crease. The conditions imposed on the polynomials are listed in table 4. While the crease can undergo twist, the faces are assumed to be inflexible; displacement polynomials are chosen such that the material properties of the face do not influence the results. As a result, the edges of the crease that are parallel to the XZ plane in a flat composite, remain straight when folded.

For a crease modulus, thickness, and width of 200 GPa, 25 μm, and 19 mm, respectively, fold angle (η) is calculated as a function of prestrain angle (θ). Figure 14 shows η for various values of the EMC's transverse modulus E_2. Fold angle increases with an increase in θ, yielding an almost flat composite at around 45°. The range of θ for fold generation, increases with a decrease in E_2. However, the tradeoff in reducing bond strength between the EMC's fibers and matrix is a non-negligible in-plane Poisson's ratio. For $0 < \theta < 45$, calculations of the slope $\partial w_0/\partial y$ of the faces revealed that the twist in the composite is negligible (not illustrated). Such a response can be attributed to three factors: high aspect ratio of the crease in the XY plane; the straight-edge condition imposed on the edges common to the crease and faces; and a high crease modulus. For $\theta = 45°$, calculations show a large angle of twist; the result corresponds to a pure twisting mode in a fold-free composite.

Fold angle can be maximized by orienting the EMC prestrain orthogonal (X axis) to the crease (Y axis). For a given fold angle, the reduction in the EMC's strain energy in the X direction due to its rotation can be compensated by increasing the prestrain. However, there may be practical limits on prestrain from a durability standpoint; minimal prestrain translates to minimal shear stress between the EMC and the constraining layer. When considering the combined effect of orientation and crease width, the range of prestrain orientations ($0 < \theta < 45$) that yield folds is found to be independent of crease width (figure 15). However, wider creases provide a higher range of foldability (η), as shown in previous results. The calculations of fold angle in figure 15 are performed for an EMC transverse modulus of 250 MPa.

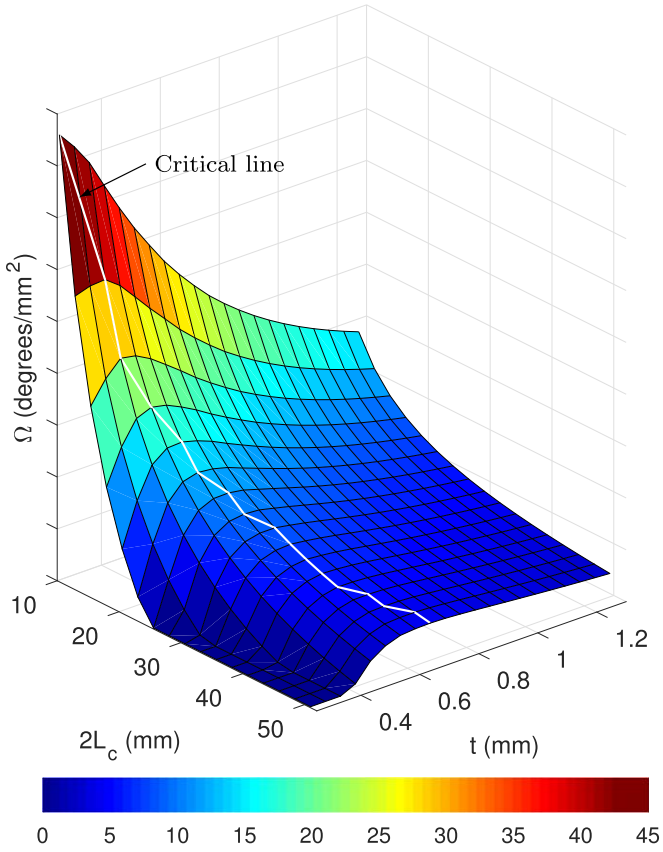

Figure 13. Fold sharpness as a function of crease width and thickness, shown for a crease modulus of 2 GPa. The critical value of fold sharpness is found as the maximum value for a given crease width.

Table 4. Conditions imposed on displacement polynomials for the modeling of folds at a crease with non-orthogonal EMC prestrain.

	Crease		Face	
	O_i	Condition	O_i	Condition
u_0	3	Terms with odd power, $u_0(0, 0) = 0$	1	Includes xy term
v_0	3	Terms with odd power, $v_0(0, 0) = 0$	1	Includes xy term
w_0	4	Terms with even power, $w_0(0, 0) = 0$	1	Includes xy term

5. Conclusions

Foldable structures address the need for creating three-dimensional objects from flat, inextensible panels and for stowing or deploying them to serve various functions. The special kinematic behaviors possible with origami folding provide possibilities for novel designs in engineering applications. The understanding created in this paper on folding laminated composites with finite thickness enables origami-inspired designs for a variety of applications including solar arrays, deployable robots, and automotive airbags. We have shown that smooth folds can be created in pre-creased laminated composites by applying mechanical prestress to select laminae. This versatile approach not only enables localized prestress application at a crease, but also allows folding at multiple non-parallel creases using a single source of prestress.

Smart laminae with controllable modulus can be locally activated to realize autonomous folding in prestressed composites. The analytical model developed in this work serves as a tool for designing folds for a given set of laminae. From model-based analyses, it is shown that narrow creases require higher input prestrain when compared to wider creases. Fold sharpness can be maximized by minimizing crease width and thickness. From an internal-energy standpoint, folding is most effective when the applied prestress is orthogonal to the crease. The EMC's anisotropy is a tradeoff between achieving zero in-plane Poisson's ratio for undirectional prestress and maximizing the range of crease orientations for foldability. The stress-biased composites presented in this work have the potential to serve as a framework for smart origami structures with reconfigurable creases.

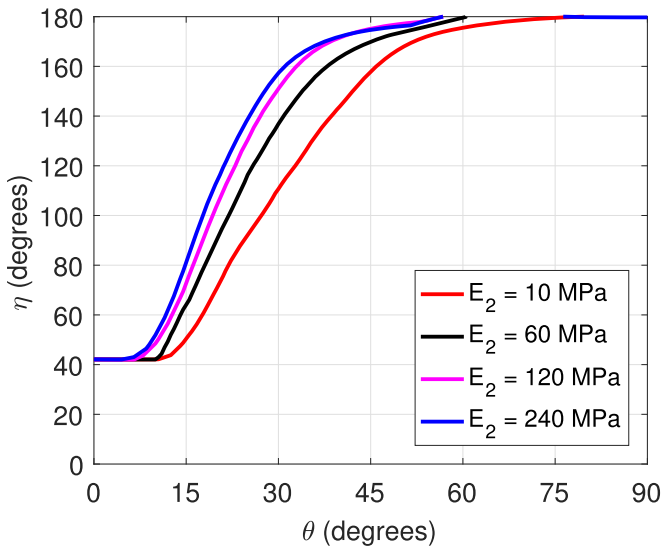

Figure 14. Fold angle as a function of prestrain angle for various values of transverse (fiber-direction) modulus of an EMC.

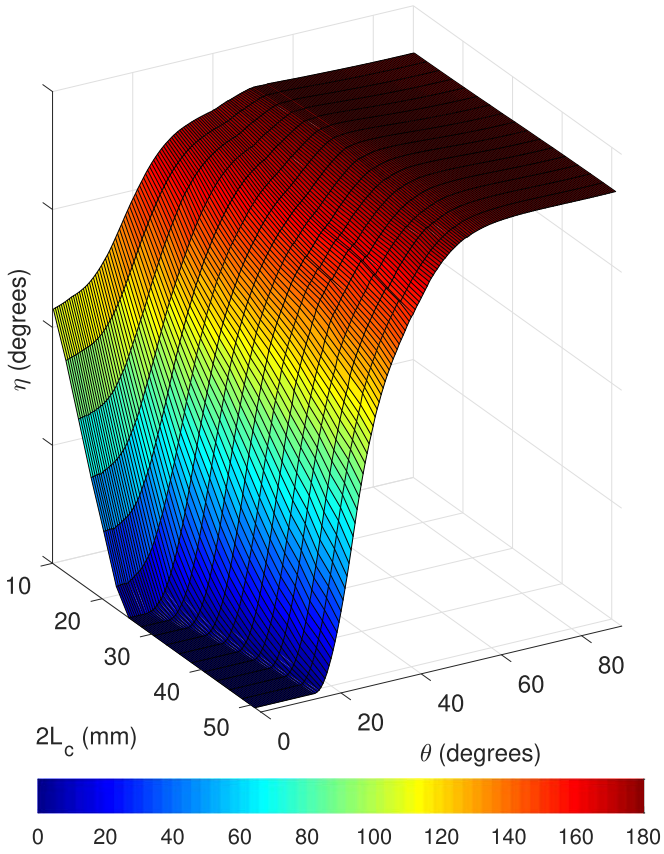

Figure 15. Fold angle as a function of prestrain angle and crease width.

Acknowledgments

Financial support was provided by member organizations of the Smart Vehicle Concepts Center, a National Science Foundation Industry-University Cooperative Research Center (www.SmartVehicleCenter.org). Additional support for VSC was provided by a Smart Vehicle Center Graduate Fellowship.

ORCID iDs

V S C Chillara https://orcid.org/0000-0001-6651-3763
M J Dapino https://orcid.org/0000-0003-4888-1903

References

[1] Zirbel S A *et al* 2013 Accommodating thickness in origami-based deployable arrays *Journal of Mechanical Design* **135** 111005
[2] Snyder M P, Sanders B, Eastep F E and Frank G J 2009 Vibration and flutter characteristics of a folding wing *J. Aircr.* **46** 791–9
[3] Cromvik C and Eriksson K 2006 Airbag folding based on origami mathematics *Origami* vol 4 (Boca Raton, FL: CRC Press) pp 129–39 978-1-4398-7104-1
[4] Felton S, Tolley M, Demaine E, Rus D and Wood R 2014 A method for building self-folding machines *Science* **345** 644–6
[5] Daynes S, Trask R S and Weaver P M 2014 Bio-inspired structural bistability employing elastomeric origami for morphing applications *Smart Mater. Struct.* **23** 125011
[6] Lang R J 1996 A computational algorithm for origami design *Proceedings of the Twelfth Annual Symposium on Computational Geometry* pp 98–105
[7] Tachi T 2009 Simulation of rigid origami *Origami* vol 4 (Boca Raton, FL: CRC Press) pp 175–87 978-1-4398-7104-1
[8] Lang R J, Tolman K A, Crampton E B, Magleby S P and Howell L L 2018 A Review of thickness-accommodation techniques in origami-inspired engineering *Appl. Mech. Rev.* **70** 010805
[9] Delimont I L, Magleby S P and Howell L L 2015 Evaluating compliant hinge geometries for origami-inspired mechanisms *Journal of Mechanisms and Robotics* **7** 011009
[10] Berbinau P, Soutis C and Guz I A 1999 Compressive failure of 0° unidirectional carbon-fibre-reinforced plastic (CFRP) laminates by fibre microbuckling *Compos. Sci. Technol.* **59** 1451–5
[11] Murphey T, Meink T and Mikulas M 2001 Some micromechanics considerations of the folding of rigidizable composite materials *In: 19th AIAA Applied Aerodynamics Conference. Fluid Dynamics and Co-located Conferences* p 1418
[12] Peraza-Hernandez E A, Hartl D J, Malak R J Jr and Lagoudas D C 2014 Origami-inspired active structures: a synthesis and review *Smart Mater. Struct.* **23** 094001
[13] Peraza-Hernandez E, Hartl D, Galvan E and Malak R 2013 Design and optimization of a shape memory alloy-based self-folding sheet *Journal of Mechanical Design* **135** 111007
[14] Felton S M *et al* 2013 Self-folding with shape memory composites *Soft Matter.* **9** 7688–94
[15] Ahmed S, Ounaies Z and Arrojado E A F 2017 Electric field-induced bending and folding of polymer sheets *Sensors and Actuators: A Physical* **260** 68–80
[16] von Lockette P and Sheridan R 2013 Folding Actuation and Locomotion of Novel Magneto-Active Elastomer (MAE) Composites *In: ASME 2013 Conference on Smart Materials, Adaptive Structures and Intelligent Systems* V001T01A020
[17] Li S and Wang K W 2015 Fluidic origami: a plant-inspired adaptive structure with shape morphing and stiffness tuning *Smart Mater. Struct.* **24** 105031
[18] Zirbel S A, Trease B P, Magleby S P and Howell L L 2014 Deployment methods for an origami-inspired rigid-foldable array *In: The 42nd Aerospace Mechanism Symposium, (NASA/CP-2014-217519)* pp 189–94 https://ntrs.nasa.gov/search.jsp?R=20150004060
[19] Emam S A and Inman D J 2015 A review on bistable composite laminates for morphing and energy harvesting *Appl. Mech. Rev.* **67** 060803
[20] Chillara V S C, Headings L M and Dapino M J 2016 Multifunctional composites with intrinsic pressure actuation and prestress for morphing structures *Compos. Struct.* **157** 265–74
[21] Chillara V S C, Headings L M and Dapino M J 2015 Self-folding laminated composites for smart origami structures *In: ASME 2015 Conference on Smart Materials, Adaptive Structures and Intelligent Systems* p 8968
[22] Kilian M, Flöry S, Chen Z, Mitra N J, Sheffer A and Pottmann H 2008 Curved folding *ACM Trans. Graph.* **27** 75:1–75:9
[23] Dureisseix D 2012 An overview of mechanisms and patterns with origami *International Journal of Space Structures* **27** 1–14
[24] Chillara V S C and Dapino M J 2017 Mechanically-prestressed bistable composite laminates with weakly coupled equilibrium shapes *Composites Part B: Engineering* **111** 251–60
[25] Murray G, Gandhi F and Bakis C 2010 Flexible matrix composite skins for one-dimensional wing morphing *Journal of Intelligent Materials Systems and Structures* **21** 1771–81
[26] Bubert E A, Woods B K S, Lee K, Kothera C S and Wereley N M 2010 Design and fabrication of a passive 1D morphing aircraft skin *Journal of Intelligent Materials Systems and Structures* **21** 1699–717
[27] Schenk M and Guest S D 2011 Origami folding: a structural engineering approach *In: Origami 5: Fifth International Meeting of Origami Science, Mathematics, and Education* (Boca Raton, FL: CRC Press) pp 291–304 978-1-4398-7350-2
[28] Hyer M W 1982 The room-temperature shapes of four-layer unsymmetric cross-ply laminates *J. Compos. Mater.* **16** 318–40
[29] Dano M L and Hyer M W 1998 Thermally-induced deformation behavior of unsymmetric laminates *Int. J. Solids Struct.* **35** 2101–20
[30] Reddy J N 1997 *Mechanics of Laminated Composite Plates: Theory and Analysis* (Boca Raton, FL: CRC Press) 9780203502808
[31] Peraza Hernandez E A, Hartl D J, Akleman E and Lagoudas D C 2016 Modeling and analysis of origami structures with smooth folds *Computer-Aided Design* **78** 93–106
[32] Mattioni F, Weaver P M and Friswell M I 2009 Multistable composite plates with piecewise variation of lay-up in the planform *Int. J. Solids Struct.* **46** 151–64
[33] Brinson L C 1993 One-dimensional constitutive behavior of shape memory alloys: thermomechanical derivation with non-constant material functions and redefined martensite internal variable *Journal of Intelligent Materials Systems and Structures* **4** 229–42
[34] Leng J, Lan X, Liu Y and Du S 2011 Shape-memory polymers and their composites: stimulus methods and applications *Prog. Mater. Sci.* **56** 1077–135
[35] Glaser R, Caccese V and Shahinpoor M 2011 Development of magneto-rheological fluid composites with rigidification characteristics *Smart Mater. Struct.* **20** 045018
[36] DeSain J, Brady B, Metzler K, Curtiss T and Albright T 2009 Tensile tests of paraffin wax for hybrid rocket fuel grains *In: 45th AIAA/ASME/SAE/ASEE Joint Propulsion Conference & Exhibit* **5115** pp 1–27